UC Davis

UC Davis Previously Published Works

Title

Wsh3/Tea4 is a novel cell-end factor essential for bipolar distribution of Tea1 and protects cell polarity under environmental stress in S. pombe

Permalink

https://escholarship.org/uc/item/2mp1j6gj

Journal

Current Biology, 15(11)

ISSN

0960-9822

Authors

Tatebe, H
Shimada, K
Uzawa, S
et al.

Publication Date

2005-06-01

Peer reviewed

eScholarship.org Powered by the California Digital Library
University of California

4/22/05

Wsh3/Tea4 is a novel cell-end factor essential for bipolar distribution of Tea1 and protects cell polarity under environmental stress in fission yeast

Hisashi Tatebe[1], Koichi Shimada[1,3], Satoru Uzawa[2] , Susumu Morigasaki[1] and Kazuhiro Shiozaki[1]*

[1]*Section of Microbiology, Division of Biological Sciences, University of California, Davis, California 95616*

[2]*Department of Biochemistry and Biophysics, University of California, San Francisco, California 94143, USA*

Running title: A novel cell polarity factor in fission yeast

*Correspondence to: Kazuhiro Shiozaki
Phone: (530) 752-3628 Fax: (530) 752-9014
E-mail: kshiozaki@ucdavis.edu

[3]Present address: Department of Periodontology, Nihon University School of Dentistry, Chiyoda-ku, Tokyo 101-8310, Japan.

Summary

Background: The fission yeast *Schizosaccharomyces pombe* has a cylindrical cell shape where growth is strictly limited to both ends, serving as an excellent model system for genetic analysis of cell polarity determination. Previous studies identified a cell-end marker protein, Tea1, which is transported by cytoplasmic microtubules to cell tips and recruits other cell-end factors, including the Dyrk-family Pom1 kinase. The Δ*tea1* mutant cells cannot grow in a bipolar fashion and show T-shaped morphology after heat shock.

Results: We identified Wsh3/Tea4 as a novel protein that interacts with Win1 MAP kinase kinase kinase (MAPKKK) of the stress-activated MAP kinase cascade. Wsh3 forms a complex with Tea1 and is transported to cell tips by growing microtubules. The Δ*wsh3* mutant shows monopolar growth with abnormal Tea1 aggregate at the non-growing cell end, which fails to recruit Pom1 kinase. Consistent with the observed interaction between Win1 and Wsh3, cells lacking Wsh3 or Tea1 show severer cell polarity defects under osmolarity and heat stress stimuli that are known to activate the stress MAPK cascade. Furthermore, mutants of the stress MAPK also exhibit cell polarity defects when exposed to the stress.

Conclusions: Wsh3/Tea4 is an essential component of the Tea1 cell-end complex. In addition to its role in bipolar growth during the normal cell cycle, the Wsh3–Tea1 complex contributes to cell polarity maintenance under stress conditions, together with the stress-signaling MAPK cascade.

Introduction

A eukaryotic intracellular signaling module, the mitogen-activated protein kinase (MAPK) cascade, transmits signals through sequential activation of three tiers of protein kinases, MAPK kinase kinase (MAPKKK), MAPK kinase (MAPKK) and MAPK [1]. In a number of signal transduction pathways from yeast to humans, MAPK cascades link cell surface receptors to nuclear transcription factors, regulating gene expression in response to extracellular stimuli [2-4]. Although less well characterized, MAPKs also controls cytoplasmic processes. For example, phosphorylation of the myosin light chain kinase (MLCK) by MAPK in the cytoplasm is believed to regulate cell motility [5]. Another striking example for non-nuclear functions of MAPK is that the JIP (JNK Interacting Protein) scaffold proteins, which tether the stress-activated MAPK cascades, are transported away from the nucleus by kinesin, a plus end-directed microtubule motor protein [6, 7]. In developing neurons, JIP proteins transported along the microtubules accumulate at the tips of extending neurites [8-10]. Studies of JIP-deficient animals suggest that JIP proteins play roles in axonal vesicle transport and morphogenesis of the nervous systems [11, 12].

The fission yeast *Schizosaccharomyces pombe* has a cylindrical cell shape, which is maintained through exclusive tip growth [13]. This highly polarized cell morphology is established by cytoplasmic microtubules that emanate from microtubule organizing centers (MTOCs) on the nuclear envelope, extending toward both cell tips [14-16]. Plus ends of growing microtubules carry the cell-end marker protein, Tea1, and, once they reach cell tips, Tea1 is deposited to the cell cortex, establishing the specific bipolar localization of Tea1 [17]. The cell-end localization of Tea1 is also dependent on the Tea2 kinesin [18], a microtubule plus end-tracking protein called Tip1 [19], as well as the Mod5 protein, which is anchored to the cell-tip plasma membrane through its C-terminal lipid modification [20]. Gel filtration and density-gradient centrifugation

experiments suggest that Tea1 forms multiple high-molecular weight protein complexes, with other proteins that also function at cell tips [17, 21]. Loss of the Tea1 protein complexes in the Δ*tea1* mutant results in mislocalization of other cell-end factors, such as Tea3 [22], Bud6/Aip3 [23, 24], and a Dyrk-family protein kinase, Pom1 [25].

Although absence of Tea1 does not lead to the loss of the cylindrical cell morphology, the Δ*tea1* mutant is often bent and grows only in a monopolar fashion, in contrast to bipolar growth of wild-type cells [17]. It was also reported that the cell polarity defect of Δ*tea1* is exacerbated after a heat shock by shifting the culture temperature from 25^{o}C to 36^{o}C, leading to T-shaped morphology [17]. These observations imply that Tea1 may play a role under certain stress conditions, in addition to its function during the normal cell cycle.

Here, we report a novel cell-end protein in *S. pombe*, Wsh3/Tea4, which is transported to cell tips by forming a complex with Tea1 and essential for formation of the functional Tea1 complex at cell tips. Strikingly, we isolated Wsh3 in a yeast two-hybrid screen for its interaction with Win1 MAPKKK of the stress-activated Spc1 MAPK cascade. Spc1 [26], also known as Sty1 [27], is a structural, functional ortholog of the mammalian stress MAPKs, such as p38 and JNK, and responsive to diverse forms of environmental stress, including high osmolarity and heat shock [28, 29]. Indeed, the cell branching phenotypes in the Δ*wsh3* and Δ*tea1* mutants are significantly accentuated after heat shock and high osmolarity, stress stimuli that activate the Spc1 MAPK cascade. We propose that, in addition to its role in bipolar cell growth, the Tea1-Wsh3 complex contributes to the maintenance of cell polarity under stress conditions that affects the cytoskeleton.

Results

Isolation of Wsh3 as a Novel MAPKKK-interacting Protein

Aiming to discover proteins that regulate the activity and/or function of the stress-responsive Spc1 MAPK cascade, we searched for proteins interacting with the non-catalytic domain of Win1 MAPKKK [30] by yeast two-hybrid screens. This screen repeatedly isolated cDNA clones containing an open reading frame SPBC1706.01, which we named *wsh3*$^{+}$ (Win1-interacting SH3-domain protein). Wsh3 is a 809-amino acid, 89.5-kDa protein with a Src homology 3 (SH3) domain at residues 121-178, as well as a cluster of acidic amino acid residues at 81-99 (Figure 1A). Database search indicated that Wsh3 shares a weak sequence similarity with the budding yeast Bud14, which is involved in bipolar bud site selection [31, 32]. Other published fungal genome sequences also contain potential orthologs (data not shown).

Interaction between Win1 MAPKKK and Wsh3 was also detected biochemically in *S. pombe*. Wsh3 was overexpressed from a plasmid with a N-terminal GST (glutathione *S*-transferase) tag, and isolation of GST-Wsh3 by glutathione-Sepharose led to co-precipitation of Win1 both before and after high osmolarity stress that activates the Spc1 MAPK cascade (Figure 1B). However, despite repeated attempts, we failed to detect significant co-purification of the endogenous Wsh3 and Win1 proteins (data not shown); their physical association may not be strong enough to survive protein dilution during cell lysate preparation.

The *wsh3* Mutant Shows Cell Polarity Defects Accentuated by Stress Conditions

To examine the cellular function of Wsh3, the *wsh3* null (Δ*wsh3*) strain was constructed by the gene disruption technique. The haploid Δ*wsh3* mutant was found to be viable with a doubling time similar to *wsh3*$^{+}$ strains (data not shown). We quantified Spc1 MAPK activation under different stress conditions by immunoblotting with the antibodies that specifically crossreact with the phosphorylated, active Spc1 [33]. Spc1 activation in Δ*wsh3* cells was comparable to that in wild-type cells, suggesting that Wsh3 does not

affect the stress activation of Win1 MAPKKK for signaling to Spc1 MAPK (data not shown).

However, under stress conditions, Δ*wsh3* cells showed significant morphological defects. After shifting to high osmolarity medium containing 0.6 M KCl or 1 M sorbitol, 20~30% of Δ*wsh3* cells exhibited highly bent or branched morphology (Figure 2A). Heat shock treatment by shifting cultures from 25°C to 36°C also had similar effects on the Δ*wsh3* morphology. On the other hand, oxidative stress by hydrogen peroxide, which also induces Spc1 activation [34], did not significantly affect Δ*wsh3* cells (data not shown). These observations indicate that Wsh3 function is important to maintain the growth polarity under high osmolarity stress and heat shock, and the loss of Wsh3 leads to initiation of an abnormal growth site.

The aberrant cell morphology of the Δ*wsh3* mutant resembles the reported cell polarity defects of *tea* mutants, which were isolated for their T-shaped morphology [35, 36]. The branching phenotype of the *tea* mutants is dramatically enhanced in the *cdc11* cytokinesis mutant, which repeats nuclear division cycles without cytokinesis [36]. We also found that the Δ*wsh3* mutation induced cell branching at a high frequency in the *cdc11* background after shifting-up to its restrictive temperature (Figure 2B). In early G2, *S. pombe* cells switch from monopolar to bipolar growth, a process known as NETO (New End Take Off) [37]. However, like *tea1* mutants [36], Δ*wsh3* cells were found to grow exclusively in a monopolar fashion. Actin patches, which are localized to the growing tips of fission yeast cells [38], were detected mostly in one tip of the Δ*wsh3* cell (Figure 2C). This observation was further confirmed using the *cdc25*-22 mutant that arrests in late G2 and continues bipolar growth with actin patches at both cell tips (Figure 2C, middle panel). On the other hand, the *cdc25*-22 Δ*wsh3* cells exhibited monopolar growth and actin patches were mostly concentrated to one cell tip, although some actin patches showed depolarized localization (bottom panel). Time-lapse

observation of growing Δ*wsh3* cells (Figure 2D) demonstrated that dividing daughter cells initiated cell growth at either old or new ends and continued monopolar growth.

Wsh3 Forms a Complex with the Cell-end Marker Protein Tea1

Because of the observed role of Wsh3 in the growth polarity, we examined the cellular localization of Wsh3 by tagging the chromosomal *wsh3*$^{+}$ gene with the green fluorescent protein (GFP) sequence (Figure 3A). The majority of Wsh3-GFP was concentrated at both cell tips and also observed as dots in the cytoplasm. In dividing cells, the Wsh3-GFP signal was also detected as a medial band (Figure 3A, right panel). These specific localization patterns of Wsh3 appeared to be dependent on cellular microtubules, because the cell-end localization of Wsh3-GFP was abrogated by a mutation in β-tubulin, *nda3-KM311* [39] even at its permissive temperature, 30^{o}C (Figure 3B, left). Consistently, treatment with microtubule inhibitors, thiabendazole (TBZ) and methyl benzimidazol-2yl carbamate (MBC), significantly reduced accumulation of Wsh3-GFP at cell tips (data not shown).

The localization pattern of Wsh3 and its microtubule-dependency is very similar to those of the cell-end marker protein Tea1, which is localized at plus ends of growing microtubules and deposited at cell tips [17, 20, 40]. Indeed, by using a strain that co-expresses the GFP-fused α tubulin and Wsh3 fused to the red fluorescent protein (RFP) [41], we observed Wsh3-RFP localized at the tip of growing microtubules was transported toward cell ends (Figure 3B, right). To further characterize the behavior of Wsh3-GFP in living cells, a newly developed microscope system (named OMX) by John W. Sedat and David A. Agard was employed (Experimental Procedures). In the OMX system, as one 3D data acquisition modality, during each exposure, the sample stage of the microscope is moved in a linear fashion along the Z-axis as a focus sweep through the thickness of samples (typically 3-5 μm for fission yeast cells), so that all signals throughout the cell are projected as one 2-dimensional image. Each 2D image was

deconvolved by computation [42]. OMX allows rapid data acquisition at close time points (50-msec exposure at one projection/sec throughout this study). Using this system, the Wsh3-GFP localization in living *S. pombe* cells was captured every second over 10 min (supplemental movie 1). To trace the movement of individual Wsh3-GFP dots over time, the movie was converted to a stereo kymograph image shown in Figure 3C. Most of Wsh3 dots appeared around the middle of the cell and moved toward cell tips at average ~3 μm/min, a speed similar to that of the Tea1 dot movement [40].

Furthermore, we found that the normal Wsh3 distribution is dependent on Tea1. The specific localization of Wsh3-GFP was lost in the Δ*tea1* mutant and the Wsh3-GFP signal was diffused throughout the cytoplasm (Figure 4A). These results suggest that Wsh3 is localized at cell tips and cytoplasmic dots through its binding to Tea1. Consistent with this model, association between the Wsh3 and Tea1 proteins in cell lysate was detected by co-precipitation experiments (Figure 4B). Furthermore, significant overlaps of cellular localization of Wsh3 and Tea1 were confirmed using a *tea1:GFP* strain in which the chromosomal *wsh3*$^{+}$ gene was tagged with the RFP sequence (Figure 4C).

Taken together, these results strongly suggest that Wsh3 forms a complex with Tea1 and is transported to cell tips by the cytoplasmic microtubule system in a Tea1-dependent manner.

Wsh3 Is Essential for Bipolar Localization of the Cell-end Marker Tea1 and the Pom1 Protein Kinase

To further characterize the role of Wsh3 in cell polarity determination, we tested whether Wsh3 affects the localization of Tea1 (Figure 5A). In the *wsh3*$^{+}$ cells, Tea1-GFP was clearly observed at both cell tips as reported previously [17]. In contrast, most of Δ*wsh3* cells showed highly concentrated Tea1-GFP signals at one end, while the other end contained significantly less Tea1-GFP dots (Figure 5A, right panel). Because the Δ*wsh3*

mutant grows in a monopolar fashion (Figure 2), we examined whether this biased Tea1 localization correlates with the tip growth pattern of Δ*wsh3* cells; concentrated actin patches and the Tea1-GFP accumulation were localized at opposite ends of Δ*wsh3* cells (Figure 5B). Thus, the Tea1-accumulating tip of Δ*wsh3* cells is not capable of growth.

Live cell imaging of Tea1-GFP with the OMX system (Figure 5C) showed that, in wild-type cells (supplemental movie 2), Tea1 dots appeared around the middle of the cell and moved toward both cell tips (Figure 5C, left panels), as previously reported [17, 40]. The kymograph expanded for the tip region (Figure 5C [i]) shows that the Tea1-GFP pattern altered with time, suggesting the dynamic nature of the cell-end structure containing Tea1. This was in clear contrast with the kymograph of the Tea1-accumulating cell tip of the Δ*wsh3* strain (Figure 5C [v]); very little change was observed during the experiment except gradual photobleaching. Transport of Tea1-GFP dots to the opposite end of the Δ*wsh3* cell was also observed (Figure 5C [iv] and supplemental movie 3), but these dots often disappeared after they reached the cell tip and never accumulated to the levels observed in wild-type cells (Figure 5C [iii]).

Pom1 is a member of the Dyrk family protein kinase and localized at cell tips in a Tea1-dependent manner [25]. In the Δ*wsh3* cells, the cell-end localization of Pom1 was lost and Pom1-GFP often accumulated in vesicle-like structures in the cytoplasm (Figure 5D). Immunoblotting analysis indicated that the Pom1 protein level was not significantly altered between wild-type and Δ*wsh3* strains (data not shown). These results suggest that the Tea1-containing structures at cell tips of Δ*wsh3* are not functional and cannot recruit Pom1 kinase. Consistently, the Δ*wsh3* defects described above (Figure 2) are very similar to the phenotypes of Pom1-defective strains [25, 43]; both Δ*wsh3* and Δ*pom1* mutants show monopolar growth and their branching morphology is enhanced in the *cdc11* background. We also observed branched cell morphology with the Δ*pom1* strain after osmostress and heat shock (data not shown). In

addition, their division septum is often misplaced from the center of the cell (Figure 5E). These observations strongly suggest that the Pom1 kinase is not functional in the Δ*wsh3* mutant. Consistently, the Δ*wsh3* Δ*pom1* double mutant exhibited stress-induced morphological defects similar to those of the Δ*wsh3* single mutant (data not shown). On the other hand, cellular localization of Wsh3-GFP appeared to be normal in Δ*pom1* cells, indicating that the Pom1 function is not required for the proper localization of Wsh3 (data not shown).

Wsh3, Tea1 and Spc1 MAPK Contribute to Cell Polarity Maintenance under Stress Conditions

As described above, Wsh3 interacts with Win1 MAPKKK of the stress MAPK cascade and the Δ*wsh3* mutant shows cell polarity defects, which are accentuated by stress stimuli that activate the MAPK cascade. Because Wsh3 forms a complex with Tea1, we examined whether the Tea1 function is also important under the stress conditions. It was previously reported that Δ*tea1* cells exhibit branching at high frequency after the temperature shift from 25^{o}C to 36^{o}C (Figure 6A; [17, 20, 44]). We found that high osmolarity stress by 0.6 M KCl also promotes appearance of T-shaped cells in the Δ*tea1* strain, to the levels comparable to the Δ*wsh3* mutant (Figure 6B). The Δ*wsh3* Δ*tea1* double and Δ*wsh3* Δ*tea1* Δ*pom1* triple mutants exhibited T-shaped morphology at slightly higher frequencies than the Δ*tea1* and Δ*wsh3* single mutants under the stress conditions. These results suggest that the Tea1-Wsh3 complex plays a role in maintaining growth polarity under osmostress and heat shock.

To assess the involvement of the Spc1 MAPK cascade in cell polarity maintenance under stress conditions, the morphology of Δ*spc1* cells was examined under various stress conditions. Spc1 is essential for cellular survival of stress through transcriptional induction of resistance genes, and the Δ*spc1* mutant ceases cell growth and loses viability under stress conditions [26, 27, 45]. Because expression of cell

polarity phenotypes requires cell growth, we chose mild stress conditions that allowed cell growth of the Δ*spc1* mutant. Cell polarity defects with bent and branched morphology were observed after shifting the Δ*spc1* mutant from 25^{o}C to 36^{o}C (Figure 6C). We also found that, even under the optimal growth condition, the Δ*spc1* mutation exacerbates the morphology defects of the Δ*tea1* mutant; the Δ*tea1* Δ*spc1* double mutant grown at 30^{o}C in rich YES medium contain large fractions of significantly bent and branched cells (Figure 6D).

These observations suggest that, together with Wsh3-Tea1 complex, the Spc1 MAPK cascade contributes to cell polarity maintenance, particularly under osmostress and heat shock conditions.

Discussion

In this paper, we have identified a novel SH3-domain protein, Wsh3, which forms a complex with the Tea1 cell-end marker protein and is required for the proper Tea1 distribution and function; a new gene name, *tea4*$^{+}$, was recently reserved for *wsh3*$^{+}$ in the *S. pombe* GeneDB (http://www.genedb.org/genedb/pombe/index.jsp). Wsh3/Tea4 was isolated through its interaction with the stress MAPKKK, Win1. Indeed, both Δ*wsh3* and Δ*tea1* mutants exhibit cell branching under high osmolarity and heat shock conditions, indicating that the Wsh3/Tea4-Tea1 complex is required for maintaining cell polarity under environmental stress.

Both cytological and biochemical data strongly suggest that Wsh3/Tea4 binds to Tea1 and the complex is transported to cell tips by growing microtubules. On the other hand, in the Δ*wsh3* mutant, cytoplasmic dots of the Tea1-GFP are transported toward cell tips, but fail to accumulate at one cell end and form an abnormal static aggregate at the other end. Therefore, Wsh3/Tea4 is not required for the localization of Tea1 to microtubule plus ends but plays an essential role to build functional Tea1-containing structures in a bipolar fashion. Consistently, Pom1 kinase, which is anchored to cell tips in a Tea1-dependent manner [25], cannot localize properly in the Δ*wsh3* mutant. This Dyrk family protein kinase is a major determinant of the tip-directed cell growth, and the Δ*pom1* mutant is defective in bipolar growth and septum positioning [25, 46]. These phenotypes are very similar to those of Δ*wsh3*, indicating that mislocalization of Pom1 in Δ*wsh3* cells results in the loss of the Pom1 function. Together, data presented in this paper establish that Wsh3/Tea4 is a novel cell polarity factor essential for the bipolar localization and function of the cell-end marker, Tea1.

Although Wsh3-Win1 interaction was reproducibly detected by both yeast 2-hybrid and GST-Wsh3 pull-down experiments, concentrated localization of Win1 or Wis4 MAPKKKs to cell tips is not detectable (our unpublished results). Therefore, the

Wsh3/Tea4-Win1 interaction may be transient or Wsh3/Tea4 may recruit only a small subpopulation of the MAPKKK to the Tea1 complex. The following observations further corroborate a link between the Wsh3/Tea4–Tea1 complex and the Spc1 MAPK cascade. A temperature shift from 25°C to 36°C significantly increases the frequency of cell branching in both Δ*tea1* and Δ*pom1* mutants [17, 25]. We found that not only heat shock but also high osmolarity stress accentuates the cell polarity defects in the Δ*tea1* and Δ*pom1* mutants, as in the Δ*wsh3* mutants. These mutants also exhibit severe polarity defects when they exit the stationary phase and resume cell growth [20] (data not shown). Importantly, all of these conditions, heat shock, high osmolarity and recovery from the stationary phase, induce activation of the Spc1 MAPK cascade [26, 27, 34] (our unpublished results). Moreover, the Δ*spc1* mutant itself shows bent and branched cell morphologies under mild stress conditions. In addition, the Pyp1 tyrosine phosphatase, which dephosphorylates and inactivates Spc1 MAPK [26, 27], suppresses *orb4* and *orb12*, cell polarity mutants that exhibit a round cell shape [36]. Together with the detected Wsh3–Win1 MAPKKK interaction, these results suggest that the Tea1–Wsh3/Tea4 complex and the stress MAPK cascade play important roles in cell polarity maintenance under stressful conditions. It is conceivable that the Wsh3/Tea4–recruited Spc1 cascade modulates the Tea1 complex through phosphorylation, because Δ*wis1* and a mutant expressing a catalytically inactive Spc1 MAPK show cell morphology defects similar to those of Δ*spc1* cells (our unpublished results). Exact molecular function of Spc1-dependent phosphorylation in cell polarity has not been determined; the Δ*spc1* mutation affects neither the Wsh3/Tea4-Tea1 association nor their cell-end accumulation both before and after stress (our unpublished results). Identification of the direct Spc1 substrate in this context will be necessary to understand the exact role of the MAPK in cell polarity.

Previous studies indicated that Tea1, Pom1 and other cell-end factors are required for the establishment of growth sites during the normal cell cycle; mutants

lacking these proteins are unable to initiate a second growth site for bipolar growth [13, 47]. Why do the Tea1-Wsh3/Tea4 complex and the stress MAPK cascade become important under stress conditions? One likely possibility is that environmental stress has significant impacts on the cytoskeleton and therefore, cells require active adaptation mechanisms to protect or reorganize the polarized cytoskeletal structures. It is known that high osmolarity stress induces disassembly of the actin cytoskeleton [48, 49]. We also observed that, after osmostress, the dynamic polymerization/depolymerization cycle of microtubules is almost completely stalled, a dramatic change detectable only by time-lapse observation of living cells (Supplemental data). Dynamic instability is a built-in characteristic of microtubules with continuous polymerization and depolymerization, and the static microtubule structures in osmostressed cells are quite unexpected. Although the mechanism for this transient loss of microtubule dynamics is currently unknown, such a dramatic change is likely to affect the cell polarity machinery, considering the central role of the microtubule system in the establishment of growth sites in *S. pombe*.

A recent study of the mutant mice lacking JNK1 suggests that the mammalian stress MAPK is involved in microtubule dynamics of neuronal cells, in addition to its role in regulation of the c-Jun transcription factor in the nucleus [50]. The involvement of the stress-responsive MAPK in linking extracellular environment to cellular cytoskeleton may be evolutionarily conserved, with some variations specific to organisms. Because of its genetic tools and ease of microtubule studies, fission yeast is expected to serve as an excellent model to study the interaction of the stress MAPK cascade with the cytoskeletal systems.

Acknowledgments

We are grateful to J. Sedat for allowing us to use the OMX system, R. Maximo, G. Lam, J. Rust, and P. Novy for technical assistance, K. Nakano for advice, and J. Sedat and A. Ikner for critical reading of the manuscript. P. Nurse, M. Yanagida, T. Toda, T. Matsumoto, D. Hirata, K. Sawin, N. Rhind and R. Tsien kindly provided strains and plasmids. H.T. was a recipient of the JSPS (Japan Society for the Promotion of Science) Postdoctoral Fellowship for Research Abroad and the Uehara Memorial Foundation Postdoctoral Fellowship. This research was supported by a NIH grant (GM59788) awarded to K.S.

Experimental Procedures

Yeast Strains and General Techniques.

S. pombe strains used in this study are listed in Table S1. Detailed procedures for strain construction are described in Supplemental Data. Growth media and basic techniques for *S. pombe* have been described [51]. *S. pombe* cells were grown in yeast extract medium YES and synthetic medium EMM. Stress treatments of *S. pombe* cultures have been described previously [33]. TBZ (Sigma) and MBC (Sigma) were used at a final concentration of 100μg/ml and 25μg/ml, respectively.

Yeast Two-hybrid Screen

The *win1*$^+$ sequence has a pair of repetitive sequences, which prevents amplification in *E. coli* [30]. Therefore, we introduced two silent mutations at 1278 (T→G) and 1281 (A→G) in *win1*$^+$ and cloned the fragment encoding amino acid residues 282-1123 into pGBT8 to express as a fusion with the Gal4 DNA-binding domain (pGBT8-Win1N). Using a *S. pombe* cDNA library in pGADGH and a budding yeast strain HF7c [52], ~1.0x10^8 transformants were screened by histidine prototrophy and ß-galactosidase

assay. A HF7c strain carrying pGBT8-Win1N and the pGADGH vector as well as that carrying the pGBT8 vector and the pGADGH-Wsh3 were histidine auxotroph, confirming the specificity of the Win1–Wsh3 interaction in the two-hybrid assay.

Protein Co-precipitation Experiments

For GST pull-down experiments, cells carrying the pREP1KZ-Wsh3 (GST-Wsh3) plasmid were grown in EMM liquid medium lacking thiamine at 30°C for 12 hr to induce expression of GST-Wsh3 proteins. Cells were suspended in GST lysis buffer (50 mM Tris-HCl [pH8.0], 5 mM EDTA, 400 mM NaCl, 10% glycerol, 0.1 mM Na_3VO_4, 1 mM ß-mercaptoethanol, 0.5% TritonX-100) containing protease inhibitors, and lysed by vortexing with glass beads, followed by centrifugation. The soluble crude lysate was incubated with Glutathione Sepharose 4B (Amersham Biosciences) at 4°C for 30min. Immunoblotting was performed with mouse monoclonal anti-*myc* antibodies (9E10, BAbCO) and rabbit polyclonal anti-GST antibodies.

For affinity purification of the TAP-tagged Wsh3, cells grown in YES medium were harvested and suspended in IP buffer (50 mM Tris-HCl [pH7.2], 5 mM EDTA, 150 mM NaCl, 10% glycerol, 50 mM NaF, 0.1 mM Na_3VO_4, 1 mM ß-mercaptoethanol, 0.5% TritonX-100) containing protease inhibitors. Cells were lysed by vortexing with glass beads, followed by centrifugation. The soluble crude lysate was incubated with IgG Sepharose 6 (Amersham Biosciences) at 4°C for 2 hr. Immunoblotting was performed with mouse monoclonal anti-HA antibodies (12CA5, Boehringer Mannheim) and rabbit polyclonal anti-GFP antibodies (sc-8334, Santa Cruz Biotechnology).

Microscopy

Experimental procedures with the OMX optical microscope can be found in Supplemental Data. This new microscope system will also be described in the near

future in a publication. For other microscopy, an Eclipse E600 microscope (Nikon), equipped with a 60X, oil-immersion objective lens and a digital charge-coupled device camera (Orca C4742-95, Hamamatsu), was used for data acquisition (See Supplemental Data). Openlab (Improvision) and Adobe Photoshop (Adobe Systems) were used for capturing images and figure preparation, respectively.

References

1. Widmann, C., Gibson, S., Jarpe, M.B., and Johnson, G.L. (1999). Mitogen-activated protein kinase: conservation of a three-kinase module from yeast to human. Physiol. Rev. *79*, 143-180.
2. Treisman, R. (1996). Regulation of transcription by MAP kinase cascades. Curr Opin Cell Biol *8*, 205-215.
3. Gustin, M.C., Albertyn, J., Alexander, M., and Davenport, K. (1998). MAP kinase pathways in the yeast Saccharomyces cerevisiae. Microbiol Mol Biol Rev *62*, 1264-1300.
4. Yang, S.H., Sharrocks, A.D., and Whitmarsh, A.J. (2003). Transcriptional regulation by the MAP kinase signaling cascades. Gene *320*, 3-21.
5. Klemke, R.L., Cai, S., Giannini, A.L., Gallagher, P.J., de Lanerolle, P., and Cheresh, D.A. (1997). Regulation of cell motility by mitogen-activated protein kinase. J. Cell Biol. *137*, 481-492.
6. Goldstein, L.S. (2001). Kinesin molecular motors: transport pathways, receptors, and human disease. Proc. Natl. Acad. Sci. USA *98*, 6999-7003.
7. Morrison, D.K., and Davis, R.J. (2003). Regulation of MAP kinase signaling modules by scaffold proteins in mammals. Annu. Rev. Cell Dev. Biol. *19*, 91-118.
8. Meyer, D., Liu, A., and Margolis, B. (1999). Interaction of c-Jun amino-terminal kinase interacting protein-1 with p190 rhoGEF and its localization in differentiated neurons. J. Biol. Chem. *274*, 35113-35118.
9. Yasuda, J., Whitmarsh, A.J., Cavanagh, J., Sharma, M., and Davis, R.J. (1999). The JIP group of mitogen-activated protein kinase scaffold proteins. Mol. Cell. Biol. *19*, 7245-7254.
10. Verhey, K.J., Meyer, D., Deehan, R., Blenis, J., Schnapp, B.J., Rapoport, T.A., and Margolis, B. (2001). Cargo of kinesin identified as JIP scaffolding proteins and associated signaling molecules. J. Cell Biol. *152*, 959-970.
11. Byrd, D.T., Kawasaki, M., Walcoff, M., Hisamoto, N., Matsumoto, K., and Jin, Y. (2001). UNC-16, a JNK-signaling scaffold protein, regulates vesicle transport in C. elegans. Neuron *32*, 787-800.
12. Kelkar, N., Delmotte, M.H., Weston, C.R., Barrett, T., Sheppard, B.J., Flavell, R.A., and Davis, R.J. (2003). Morphogenesis of the telencephalic commissure requires scaffold protein JNK-interacting protein 3 (JIP3). Proc. Natl. Acad. Sci. USA *100*, 9843-9848.
13. Hayles, J., and Nurse, P. (2001). A journey into space. Nat. Rev. Mol. Cell Biol. *2*, 647-656.
14. Hagan, I.M., and Hyams, J.S. (1988). The use of cell division cycle mutants to investigate the control of microtubule distribuition in the fission yeast *Schizosaccharomyces pombe.* J. Cell Sci. *89*, 343-357.
15. Drummond, D.R., and Cross, R.A. (2000). Dynamics of interphase microtubules in *Schizosaccharomyces pombe*. Curr. Biol. *10*, 766-775.
16. Sagolla, M.J., Uzawa, S., and Cande, W.Z. (2003). Individual microtubule dynamics contribute to the function of mitotic and cytoplasmic arrays in fission yeast. J. Cell Sci. *116*, 4891-4903.
17. Mata, J., and Nurse, P. (1997). tea1 and the microtubular cytoskeleton are important for generating global spatial order within the fission yeast cell. Cell *89*, 939-949.

18. Browning, H., Hayles, J., Mata, J., Aveline, L., Nurse, P., and McIntosh, J.R. (2000). Tea2p is a kinesin-like protein required to generate polarized growth in fission yeast. J. Cell Biol. *151*, 15-28.
19. Brunner, D., and Nurse, P. (2000). CLIP170-like tip1p spatially organizes microtubular dynamics in fission yeast. Cell *102*, 695-704.
20. Snaith, H.A., and Sawin, K.E. (2003). Fission yeast mod5p regulates polarized growth through anchoring of tea1p at cell tips. Nature *423*, 647-651.
21. Feierbach, B., Verde, F., and Chang, F. (2004). Regulation of a formin complex by the microtubule plus end protein tea1p. J. Cell Biol. *165*, 697-707.
22. Arellano, M., Niccoli, T., and Nurse, P. (2002). Tea3p is a cell end marker activating polarized growth in *Schizosaccharomyces pombe*. Curr. Biol. *12*, 751-756.
23. Glynn, J.M., Lustig, R.J., Berlin, A., and Chang, F. (2001). Role of bud6p and tea1p in the interaction between actin and microtubules for the establishment of cell polarity in fission yeast. Curr. Biol. *11*, 836-845.
24. Jin, H., and Amberg, D.C. (2001). Fission yeast Aip3p (spAip3p) is required for an alternative actin-directed polarity program. Mol. Biol. Cell *12*, 1275-1291.
25. Bähler, J., and Pringle, J.R. (1998). Pom1p, a fission yeast protein kinase that provides positional information for both polarized growth and cytokinesis. Genes Dev. *12*, 1356-1370.
26. Shiozaki, K., and Russell, P. (1995). Cell-cycle control linked to the extracellular environment by MAP kinase pathway in fission yeast. Nature *378*, 739-743.
27. Millar, J.B.A., Buck, V., and Wilkinson, M.G. (1995). Pyp1 and Pyp2 PTPases dephosphorylate an osmosensing MAP kinase controlling cell size at division in fission yeast. Genes Dev. *9*, 2117-2130.
28. Nguyen, A.N., and Shiozaki, K. (2002). MAPping stress survival in yeasts: From the cell surface to the nucleus. In Sensing, signaling and cell adaptation, Volume 3, K.B. Storey and J.M. Storey, eds. (Amsterdam: Elsevier Science), pp. 75-90.
29. Toone, W.M., and Jones, N. (2004). Stress responses in *S. pombe*. In The molecular biology of *Schizosaccharomyces pombe*, R. Egel, ed. (Heidelberg: Springer-Verlag), pp. 57-72.
30. Samejima, I., Mackie, S., Warbrick, E., Weisman, R., and Fantes, P.A. (1998). The fission yeast mitotic regulator *win1*$^{+}$ encodes a MAP kinase kinase kinase that phosphorylates and activates Wis1 MAP kinase kinase in response to high osmolarity. Mol. Biol. Cell *9*, 2325-2335.
31. Ni, L., and Snyder, M. (2001). A genomic study of the bipolar bud site selection pattern in Saccharomyces cerevisiae. Mol Biol Cell *12*, 2147-2170.
32. Cullen, P.J., and Sprague, G.F., Jr. (2002). The Glc7p-interacting protein Bud14p attenuates polarized growth, pheromone response, and filamentous growth in *Saccharomyces cerevisiae*. Eukaryot. Cell *1*, 884-894.
33. Shiozaki, K., and Russell, P. (1997). Stress-activated protein kinase pathway in cell cycle control of fission yeast. Meth. Enzymol. *283*, 506-520.
34. Degols, G., Shiozaki, K., and Russell, P. (1996). Activation and regulation of the Spc1 stress-activated protein kinase in *Schizosaccharomyces pombe*. Mol. Cell. Biol. *16*, 2870-2877.
35. Snell, V., and Nurse, P. (1993). Investigations into the control of cell form and polarity: the use of morphological mutants in fission yeast. Dev. Suppl., 289-299.

36. Verde, F., Mata, J., and Nurse, P. (1995). Fission yeast cell morphogenesis: identification of new genes and analysis of their role during the cell cycle. J. Cell Biol. *131*, 1529-1538.
37. Mitchison, J.M., and Nurse, P. (1985). Growth in cell length in the fission yeast *Schizosaccharomyces pombe*. J. Cell Sci. *75*, 357-376.
38. Marks, J., Hagan, I.M., and Hyams, J.S. (1986). Growth polarity and cytokinesis in fission yeast: the role of the cytoskeleton. J. Cell Sci. (Suppl.) *5*, 229-241.
39. Umesono, K., Toda, T., Hayashi, S., and Yanagida, M. (1983). Cell division cycle genes *nda2* and *nda3* of the fission yeast *Schizosaccharomyces pombe* control microtubular organization and sensitivity to anti-mitotic benzimidazole compounds. J. Mol. Biol. *168*, 271-284.
40. Behrens, R., and Nurse, P. (2002). Roles of fission yeast tea1p in the localization of polarity factors and in organizing the microtubular cytoskeleton. J. Cell Biol. *157*, 783-793.
41. Campbell, R.E., Tour, O., Palmer, A.E., Steinbach, P.A., Baird, G.S., Zacharias, D.A., and Tsien, R.Y. (2002). A monomeric red fluorescent protein. Proc Natl Acad Sci U S A *99*, 7877-7882.
42. Agard, D.A., Hiraoka, Y., Shaw, P., and Sedat, J.W. (1989). Fluorescence microscopy in three dimensions. Methods Cell Biol *30*, 353-377.
43. Bähler, J., and Nurse, P. (2001). Fission yeast Pom1p kinase activity is cell cycle regulated and essential for cellular symmetry during growth and division. EMBO J. *20*, 1064-1073.
44. Sawin, K.E., and Nurse, P. (1998). Regulation of cell polarity by microtubules in fission yeast. J Cell Biol *142*, 457-471.
45. Chen, D., Toone, W.M., Mata, J., Lyne, R., Burns, G., Kivinen, K., Brazma, A., Jones, N., and Bähler, J. (2003). Global transcriptional responses of fission yeast to environmental stress. Mol. Biol. Cell *14*, 214-229.
46. Niccoli, T., Arellano, M., and Nurse, P. (2003). Role of Tea1p, Tea3p and Pom1p in the determination of cell ends in *Schizosaccharomyces pombe*. Yeast *20*, 1349-1358.
47. Chang, F. (2001). Establishment of a cellular axis in fission yeast. Trends Genet *17*, 273-278.
48. Chowdhury, S., Smith, K.W., and Gustin, M.C. (1992). Osmotic stress and the yeast cytoskeleton: phenotype-specific suppression of an actin mutation. J. Cell Biol. *118*, 561-571.
49. Rupes, I., Jia, Z., and Young, P.G. (1999). Ssp1 promotes actin depolymerization and is involved in stress response and new end take-off control in fission yeast. Mol. Biol. Cell *10*, 1495-1510.
50. Chang, L., Jones, Y., Ellisman, M.H., Goldstein, L.S., and Karin, M. (2003). JNK1 is required for maintenance of neuronal microtubules and controls phosphorylation of microtubule-associated proteins. Dev. Cell *4*, 521-533.
51. Alfa, C., Fantes, P., Hyams, J., McLeod, M., and Warbrick, E. (1993). Experiments with Fission Yeast. A laboratory course manual (Cold Spring Harbor, NY: Cold Spring Harbor Press).
52. Feilotter, H.E., Hannon, G.J., Ruddell, C.J., and Beach, D. (1994). Construction of an improved host strain for two hybrid screening. Nucleic Acids Res *22*, 1502-1503.

Figure Legends

Figure 1. Wsh3 Interacts with Win1 MAPKKK.

(A) The sequence encoding residues 282–1123 within the non-catalytic extension of Win1 was used as bait in the yeast two-hybrid screen. cDNA clones encoding the C-terminal region of Wsh3 (residues 587 - 809) were repeatedly isolated in the screen for its interaction with the Win1 bait.

(B) Win1 is co-precipitated with Wsh3. *win1:myc* Δ*wsh3* strains carrying a plasmid to express either GST or GST-Wsh3 were harvested before and 10 min after high osmolarity stress by 0.6M KCl. Proteins purified by glutathione-Sepharose beads (GSH Prep) were analyzed by immunoblotting with anti-*myc* and anti-GST antibodies. Win1 shows a gel-mobility shift upon activation by osmostress.

Figure 2. Δ*wsh3* Shows Defects in Cell Polarity.

(A) Wild-type and Δ*wsh3* strains grown in YES medium were photographed before and after stress of either 0.6 M KCl for 3 hrs or a temperature shift from 25°C to 36°C for 3 hrs. Bar, 10μm.

(B) Cell polarity defect of Δ*wsh3* is accentuated in the *cdc11* background. *cdc11-132* and *cdc11-132* Δ*wsh3* strains were grown in YES medium at 25°C, followed by incubation at 36°C for 4 hr. Bar, 20 μm.

(C) Monopolar distribution of actin by the Δ*wsh3* mutation (arrowheads). Wild-type and Δ*wsh3* strains were grown at 30˚C. *cdc25-22* and *cdc25-22* Δ*wsh3* strains were grown at 25˚C, followed by incubation at 36˚C for 3.5 hr. Actin was stained with rhodamine-phalloidin. In some Δ*wsh3* cells, actin patches are scattered and not polarized (indicated by an asterisk). Bar, 10μm. Frequencies of the actin distribution patterns are shown as a graph on the right.

(D) The Δ*wsh3* mutant shows monopolar growth. Δ*wsh3* cells were grown on YES agar medium and imaged by time-lapse microscopy. [top] Two pairs of daughter cells are shown. Arrows and outlines of cells at later time points indicate growth direction of cells. Bar, 10μm. [bottom] Summary of growth end selection patterns in Δ*wsh3.* 26 samples were examined.

Figure 3. Cellular Localization of Wsh3.

(A) A wild-type strain whose chromosomal *wsh3*$^{+}$ gene is fused with the sequence encoding GFP (*wsh3:GFP*) was observed by deconvolution microscopy. Bar, 10μm.

(B) Microtubule-dependent Wsh3 transport. [left] A *nda3-KM311* strain carrying the *wsh3:GFP* allele was grown at 30°C and observed by deconvolution microscopy. [right] Time-lapse microscopy of a *wsh3:RFP* strain expressing GFP-α tubulin. Numbers indicate the times in seconds. Bars, 10 μm.

(C) Cytoplasmic Wsh3 speckles move towards cell tips. Sequential images of a single *wsh3:GFP* cell were taken at 1 sec intervals for 10 min at room temperature and converted to a stereo kymograph that displays Wsh3 speckle movements through the time course in both x- and y(perpendicular to the images)-axes (see the schematic representation on the left). The dark region in the middle corresponds to the position of the nucleus. Bar, 2 μm.

Figure 4. Wsh3 Interacts with Tea1 *in vivo*.

(A) Wsh3 is delocalized in the Δ*tea1* mutant. A Δ*tea1 wsh3:GFP* strain grown at 30°C was observed by deconvolution microscopy. Bar, 10 μm.

(B) Tea1 forms a complex with Wsh3. *tea1:GFP* and *tea1:GFP wsh3:HATAP* strains grown at 30°C were treated with high osmolarity stress of 0.6 M KCl and harvested at the indicated time points. Wsh3HATAP was purified by IgG-Sepharose, followed by

immunoblotting with anti-GFP and anti-HA antibodies. An arrowhead indicates position of Tea1GFP detected by anti-GFP antibodies.

(C) Wsh3 is co-localized with Tea1. A *wsh3:RFP tea1:GFP* strain was grown at 30°C in EMM liquid medium and a single focal plane was captured for RFP and GFP signals. Bar, 5μm.

Figure 5. Wsh3 Is Required for the Normal Tea1 Localization.

(A) Tea1 is concentrated at one end of the Δ*wsh3* cell. Wild-type and Δ*wsh3* strains carrying the *tea1:GFP* allele were grown at 30°C and observed by deconvolution microscopy. Bar, 10μm.

(B) Actin is concentrated at the Tea1-free cell tip. A Δ*wsh3 tea1:GFP* strain was stained for Tea1GFP and actin by anti-GFP antibodies and rhodamine-phalloidin, respectively. Bar, 10 μm.

(C) The behavior of Tea1GFP at cell tips in wild type and Δ*wsh3*. Sequential images of a single *tea1:GFP* cell and a single *tea1:GFP* Δ*wsh3* cell were taken at a 1-sec interval for 10 min at room temperature and converted to kymographs, which represent Tea1 dot movements in the cytoplasm. In panels [i], [iii] and [v], kymographs at cell tip regions (shown by squares on cell images above) are further spread out to show the Tea1 movements in these areas. Bar, 2 μm.

(D) Pom1 is delocalized in Δ*wsh3*. Wild-type and Δ*wsh3* strains carrying the *pom1:GFP* allele were grown at 30˚C and observed by fluorescence microscopy. Bar, 10 μm.

(E) Septum displacement in Δ*wsh3* cells. A Δ*wsh3* strain grown in YES medium was pictured by DIC microscopy. Arrowheads indicate positions of division septa.

Figure 6. Environmental Stress Exacerbates the Cell Polarity Defects of Δ*tea1*, Δ*wsh3*, and Δ*spc1* mutants.

(A) A Δ*tea1* strain was grown in YES medium at 25°C. Cells were observed 3 hr after stress of either a temperature shift from 25°C to 36°C or 0.6 M KCl. Bar, 10μm.
(B) Appearance of T-shaped cells in wild-type, Δ*tea1*, Δ*wsh3*, Δ*wsh3* Δ*tea1* and Δ*wsh3* Δ*tea1* Δ*pom1* strains was monitored 3 hr after osmostress of 0.6 M KCl and a temperature shift from 25°C to 36°C. ≥200 cells were examined in each sample.
(C) Cell polarity defect in Δ*spc1* upon heat shock. A wild type strain and a Δ*spc1* strain were grown in YES medium at 25°C, and observed for T-shaped or severely bent cells at the indicated time points after the temperature shift to 36°C. ≥150 cells were examined in each sample. Bar, 10μm.
(D) Synthetic morphological defects in the Δ*tea1* Δ*spc1* double mutant. Wild-type, Δ*spc1*, Δ*tea1* and Δ*tea1* Δ*spc1* strains were grown at 30°C in YES medium. >120 cells were examined in each sample. Bar, 10μm.

Figure

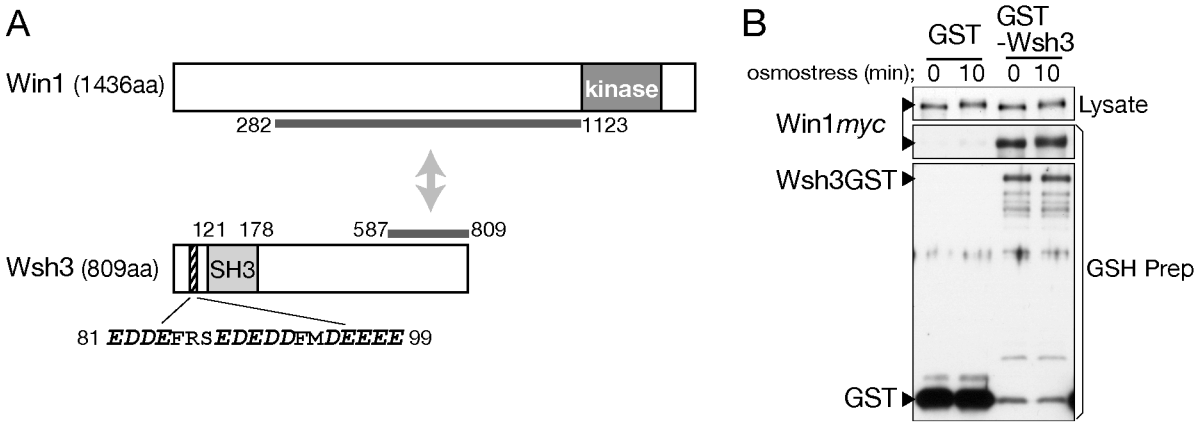


Figure-1 Tatebe *et al.*

Figure

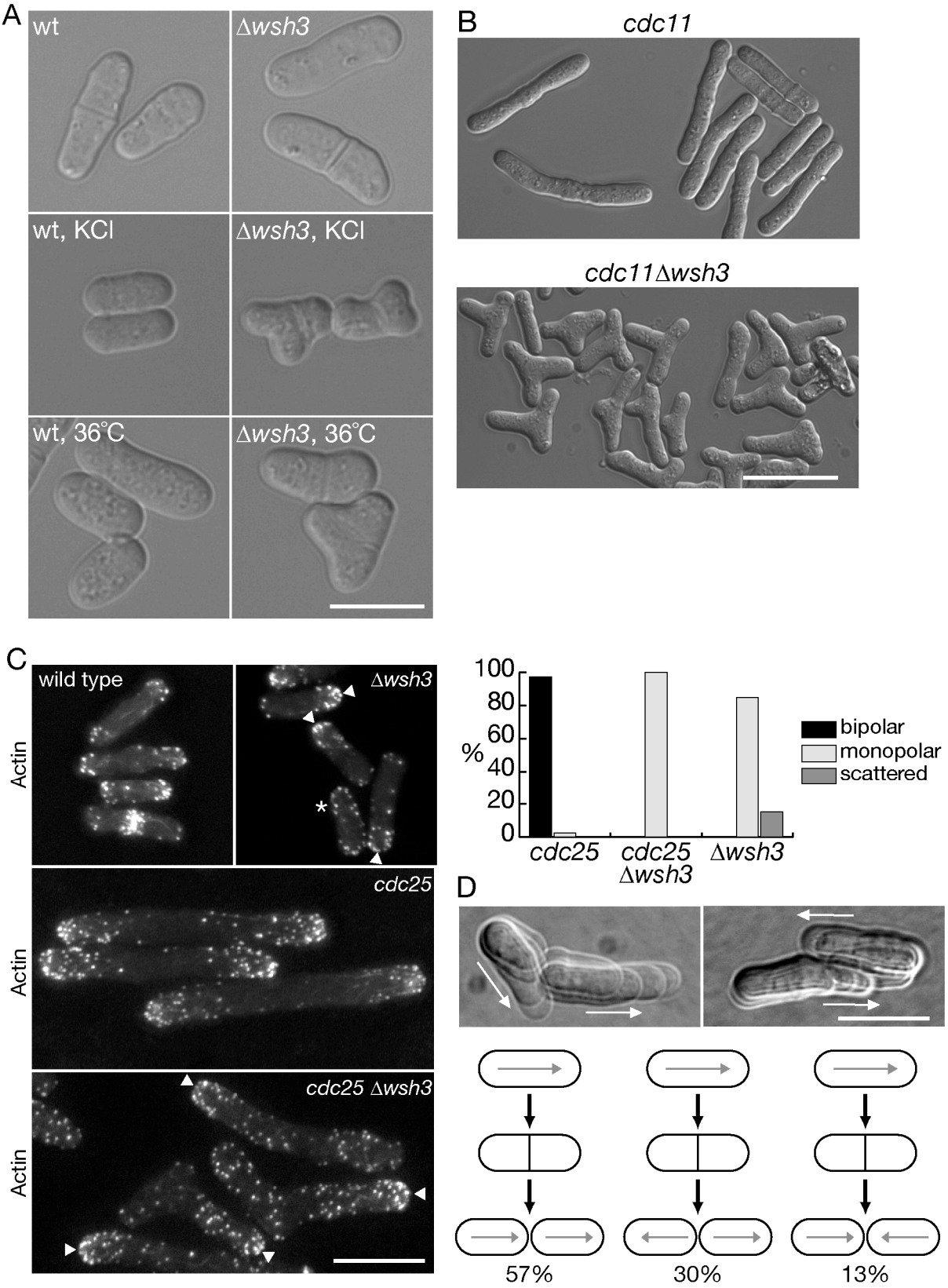


Figure-2 Tatebe *et al.*

Figure

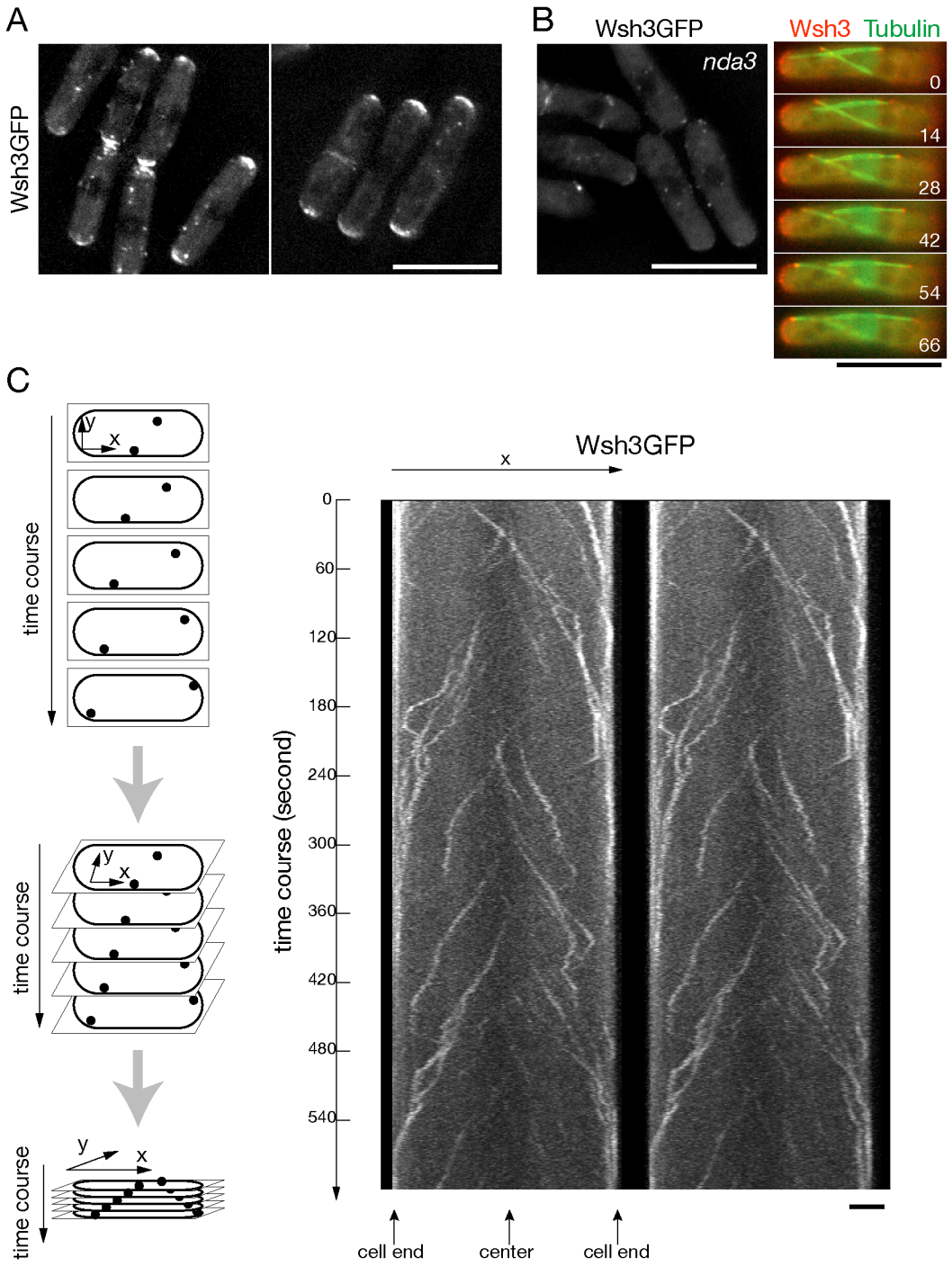


Figure-3 Tatebe *et al.*

Figure

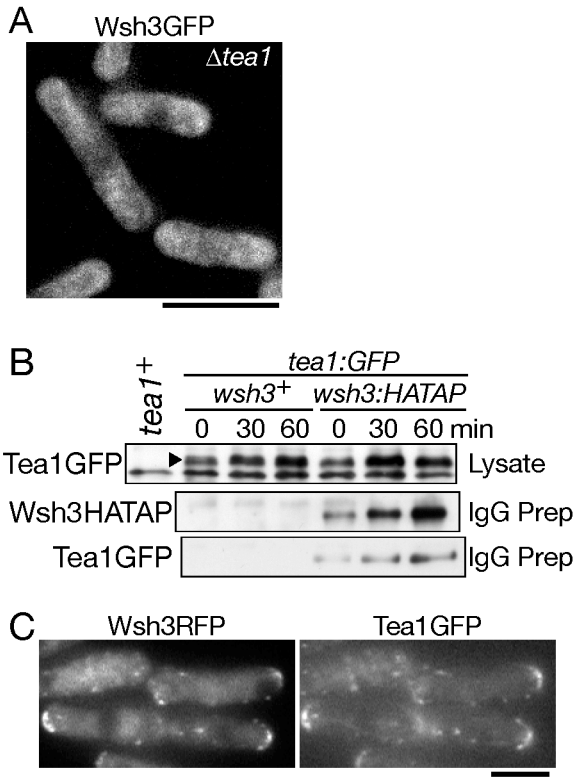


Figure-4 Tatebe *et al.*

Figure

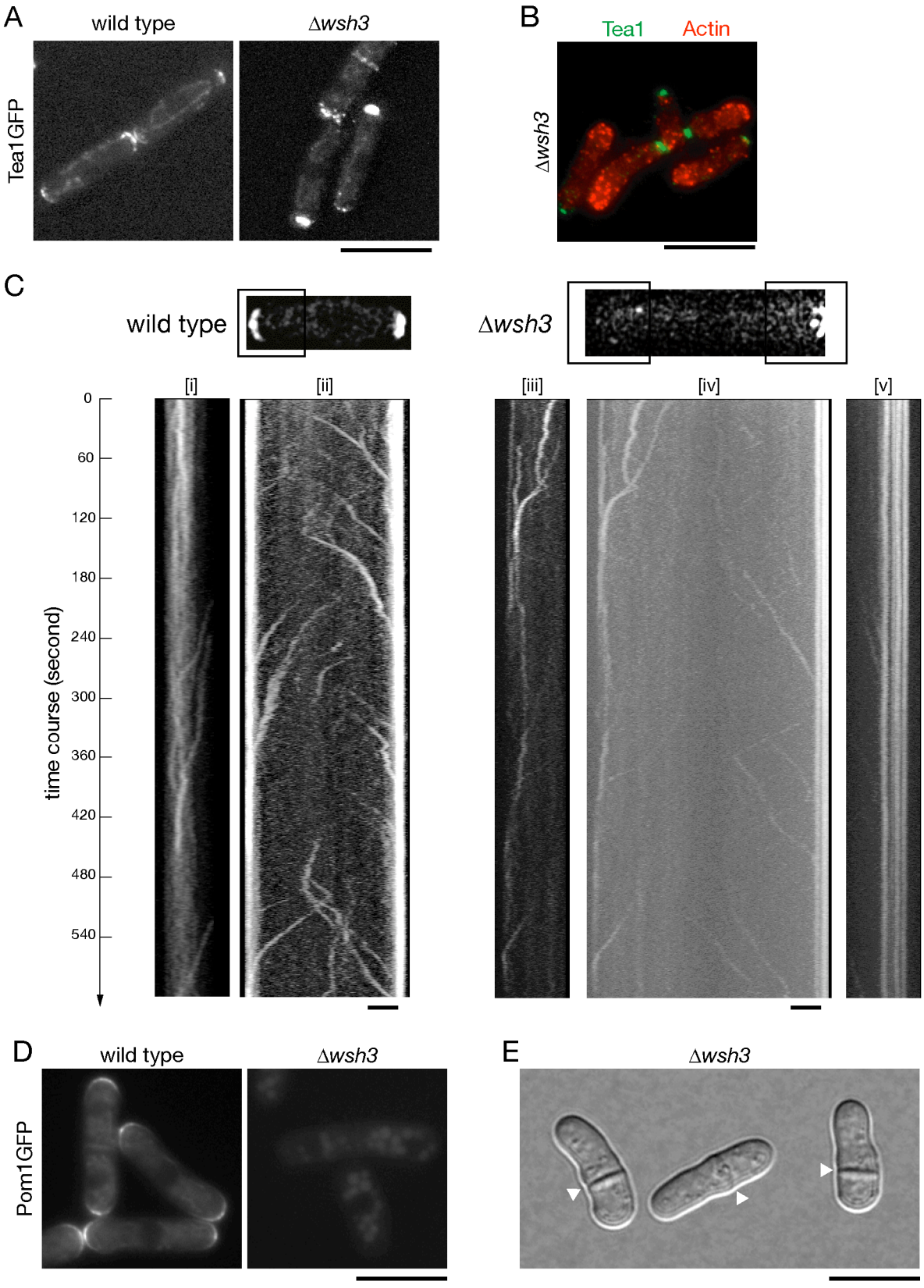


Figure-5 Tatebe *et al.*

Figure

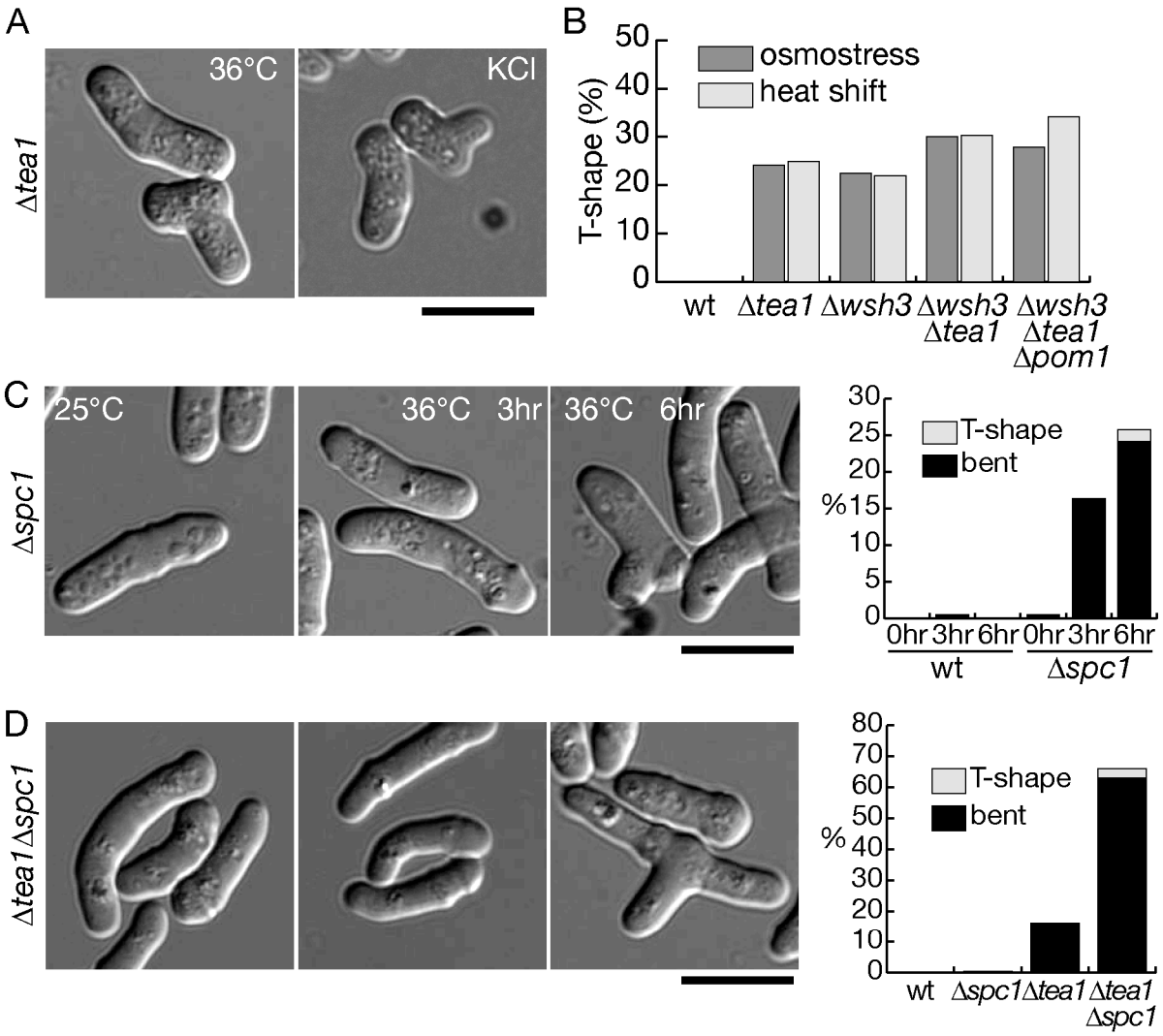


Figure-6 Tatebe *et al.*

Supplemental Materials

Supplementary Experimental Procedures

Construction of the *wsh3* Null Mutant, *wsh3:myc*, *wsh3:GFP*, *wsh3:RFP* and *wsh3:HATAP* Strains

For *wsh3* gene disruption, 0.5-kb sequences immediately upstream and downstream of the *wsh3*$^+$ open reading frame were amplified by PCR with pairs of primers (ATGCAAATACCGTACTCGCT and CGCCCTATAGTGAGTCGTATTACGCTGTCAGCACTACTGGCAC for the upstream fragment, CCTTTAGTGAGGGTTAATTAATCTTTGATTAATTTAAAAGTTATACCATG and AGAATCGCTATAAATCGTGC for the downstream fragment). The 1.8-kb *Hind*III fragment of the *ura4*$^+$ marker gene was amplified by PCR using the aforementioned 0.5-kb fragments upstream and downstream of *wsh3*$^+$ as primers. The resultant PCR product, a *ura4*$^+$ fragment flanked with the genomic sequences adjacent to *wsh3*$^+$, was used to transform a diploid strain constructed by mating haploid CA6 and CA7. Stable Ura$^+$ transformants were isolated, and the disruption of one of the *wsh3* loci was confirmed by Southern hybridization experiments, which was followed by tetrad analysis.

For constructing strains in which chromosomal *wsh3*$^+$ gene is tagged with the sequences encoding twelve copies of the *myc* epitope (myc), the green fluorescent protein (GFP) or the monomeric red fluorescent protein (mRFP1; [1]), *Not*I site was introduced by PCR at the 3'-end of the *wsh3*$^+$ sequence with an oligo DNA primer AATGCGGCCGCCGCGATTCGTATTTAAG. Digested at the 3'-end *Not*I site as well as either of the internal *BamH*I site, *EcoR*V site, or the externally added *Pst*I site at position 1904, the resultant PCR fragments were

cloned to construct pBluescript-ΔNWsh3-*myc*, pBluescript-ΔNWsh3-GFP and pBluescript-ΔNWsh3-RFP with the *ura4*$^+$ marker gene. These plasmids were used to transform a wild-type strain (PR109), and the integration of the plasmids at the *wsh3*$^+$ locus was confirmed by Southern blotting analysis. The functionality of the tagged *wsh3* alleles was confirmed by phenotypic comparison with the Δ*wsh3* strain.

For constructing a *wsh3:HATAP* strain, 0.5-kb sequences immediately upstream and downstream of the *wsh3*$^+$ stop codon were amplified by PCR with pairs of primers; ATTCTGCAGCGGCTCCATTGGAGTGTAAT and TTAATTAACCCGGGGATCCGGCGATTCGTATTTAAGAGG for the upstream fragment, CAGATCCACTAGTGGCCTATAATCTTTGATTAATTTAAAAGTTATACC and ACGAGCTCTAACCCTGTTGCCATCGAATCGTG for the downstream fragment. These fragments were used as PCR primers to amplify the HA-TAP cassette, which encodes three copies of the HA epitope followed by the TAP tag [2] as well as the *KanMX6* selection marker, using the pFS209 plasmid (a gift from Dr. N. Rhind) as template. The resultant PCR fragment was used to transform a wild-type (PR109) strain, and the integration of the fragment at the *wsh3*$^+$ locus was verified by Southern hybridization experiment. The functionality of the *wsh3:HATAP* allele was confirmed by phenotypic comparison with the Δ*wsh3* strain.

Microscopy.

To examine polarity defects, cells grown to mid-log phase were fixed in 2.5% glutaraldehyde for ≥30 min at 4°C and observed in DIC (Nomarsky differential interference contrast) microscopy. T-shaped and severely (>20°) bent cells were counted in images captured by the Openlab software (Improvision) and

statistically analyzed by Excel (Microsoft). ≥200, ≥150, and >120 cells were examined for figure-6B, 6C, and 6D, respectively. For actin staining, cells were grown to mid-log phase, followed by fixation in 3.0% formaldehyde for 30-60 min. Cell wall was digested in PEMS buffer (100 mM Pipes [pH6.9], 1 mM EGTA, 1 mM $MgSO_4$, 1.2 M Sorbitol) containing 0.6 mg/ml Zymolyase 100T (ICN Biomedicals. Inc.) for 20 min at 37°C. Each sample was incubated with 0.2 unit of rhodamine-phalloidin (Molecular Probe) in 30 µl PEM buffer (100 mM Pipes [pH6.9], 1 mM EGTA, 1 mM $MgSO_4$) for ≥1hr, followed by observing fluorescent signals. Z-axial images were taken at a 0.2-0.4 µm step and deconvolved for projection image preparation by Openlab. For double staining of actin and Tea1-GFP, cells were fixed in 3.0% formaldehyde for 30 min and cell wall was digested in PEMS buffer containing 0.6 mg/ml Zymolyase 100T for 70 min at 37°C. Samples were incubated with rabbit polyclonal anti-GFP antibodies (full-length A.v. polyclonal antibody, Clontech) for ≥16hr, followed by incubation with goat anti-rabbit antibodies conjugated with Alexa Fluor 488 (Molecular Probe) and rhodamine-phalloidin (Molecular Probe) for ≥12 hr. Z-axial images were taken at 0.4 µm steps and deconvolved for projection image preparation as described above.

For time-lapse imaging of live cells in bright field microscopy, cells were mounted on a 0.75 mm thick, YES-1.5% agarose pad, surrounded by YES liquid medium. 26 samples were examined for figure-2D. For observing GFP-fused proteins in living cells, cells were mounted on either a 0.75 mm thick, EMM-1.5% agarose pad or a thin (10-20 µm thickness), EMM-1.0% agarose film. Where indicated, Z-axial images were taken at a 0.4 µm step and deconvolved for projection images. Openlab (Improvision) and Adobe Photoshop (Adobe Systems) were used for capturing images and figure preparation, respectively. For all the experiments described above, an Eclipse E600 microscope (Nikon),

equipped with a 60X, oil-immersion objective lens and a digital charge-coupled device camera (Orca C4742-95, Hamamatsu), was used for data acquisition.

For time-lapse observation of the GFP-tagged proteins using the OMX system, cells grown to early-mid log phase in EMM with supplements were harvested and incubated for 15-30 min at room temperature in EMM containing 10 mM n-acetyl cysteine and 0.1 mM n-propyl gallate, which reduce photobleaching of GFP (S.U. and J.W. Sedat, unpublished observations). Cell suspension was spotted on an agarose pad (0.8-1% agarose in culture media) as described [3] and covered with a coverslip. For osmostress experiment, a coverslip was coated with 1 mg/ml Concanavalin A and air-dried. 50 µl of cell suspension was placed on the Concanavalin A-coated coverslip and incubated for 15 min at room temperature to allow cells to attach, followed by gentle wash with culture media to remove excess cells. After 1 min from the start of data acquisition at one projection/sec, an equal volume of the culture medium containing 1.2 M KCl, n-acetyl cysteine and n-propyl gallate was added for high osmolarity stress at 0.6 M KCl.

The OMX optical microscope, developed by the Sedat and Agard cooperative (University of California, San Francisco), is a radical newly designed system with two major goals. First, fast primarily live three-dimensional data can be acquired in several modalities (z projections using piezo technology, for example, can be collected at 30 projections/sec) at four simultaneous wavelengths; the images are collected on newly-developed back-thinned electron multiplying CCDs for highest sensitivity, important for live imaging. The data for this paper were collected on a 60x/1.2 water immersion objective and the excitation light was a 488 nm laser source, made incoherent, by appropriate optics. Secondly, the OMX microscope system allows for high resolution imaging

(= ~100 nm in x, y) using the Structure Illumination technology (see [4]). This new microscope system will be described in the near future in a publication.

Typically, the exposure time was 50 msec at one projection/second for duration of 10-15 min (600-900 images). Transmission light images for the cells before the data acquisition was taken and compared to the same field 3-6 hrs later to confirm cell growth. The resulted 2D projection was corrected for CCD gain and offset, and then deconvolved using 2D point spread function (PSF) generated from 3D PSF with projecting corresponding Z sections [5]. The deconvolution methods used were either iterative enhanced ratio method in the Prism software [6], iterative least square approach, which includes Wiener filtering. The resulted time series was presented as kymograph for data analysis as described [3].

Legends to Supplemental Figures

Supplemental Figure 1. Effects of High Osmolarity Stress on Cytoplasmic Microtubules.

Microtubule dynamics is lost upon osmostress. The *atb2:GFP* strain (CA2634) expressing the GFP:α-tubulin fusion protein was observed by the OMX system and sequential images were taken at 1 sec intervals at room temperature. Osmostress was applied by addition of KCl to the final concentration of 0.6 M at 60 sec from the start of the experiment. Images were deconvolved (Supplemental Movie 5) and converted to kymographs, representing microtubule dynamics in the cytoplasm. Bar, 2 μm.

Movie 1 Wsh3-GFP in a living wild-type cell.

A *wsh3:GFP* strain (CA2301) was mounted on EMM agarose pad, sealed under a glass coverslip. Sequential images were taken at a 1 sec interval for 10 min at room temperature and converted to a movie at 15 frames/sec.

Movie 2 Tea1-GFP in a living wild-type cell.

A *tea1:GFP* strain (CA2677) was mounted on EMM agarose pad, sealed under a glass coverslip. Sequential images were taken at a 1 sec interval for 10 min at room temperature and converted to a movie at 15 frames/sec.

Movie 3 Tea1-GFP in a living Δ*wsh3* cell.

A *tea1:GFP* Δ*wsh3* strain (CA2735) was observed as in Movie 2.

Movie 4 GFP-tubulin in a living wild-type cell.

A *atb2:GFP* strain (CA2634) was mounted on EMM agarose pad, sealed under a glass coverslip. Sequential images were taken at a 1 sec interval at room temperature and the first 7.5-min portion was converted to a movie at 15 frames/sec.

Movie 5 GFP-tubulin in a living wild-type cell upon osmostress.

A *atb2:GFP* strain (CA2634) grown in EMM liquid medium was mounted on a glass coverslip coated with concanavalin A and surrounded with EMM liquid medium. Sequential images were taken at a 1 sec interval at room temperature. KCl was added to the final concentration of 0.6 M at 60 seconds after starting data collection. The first 7.5-min portion was converted to a movie at 15 frames/sec.

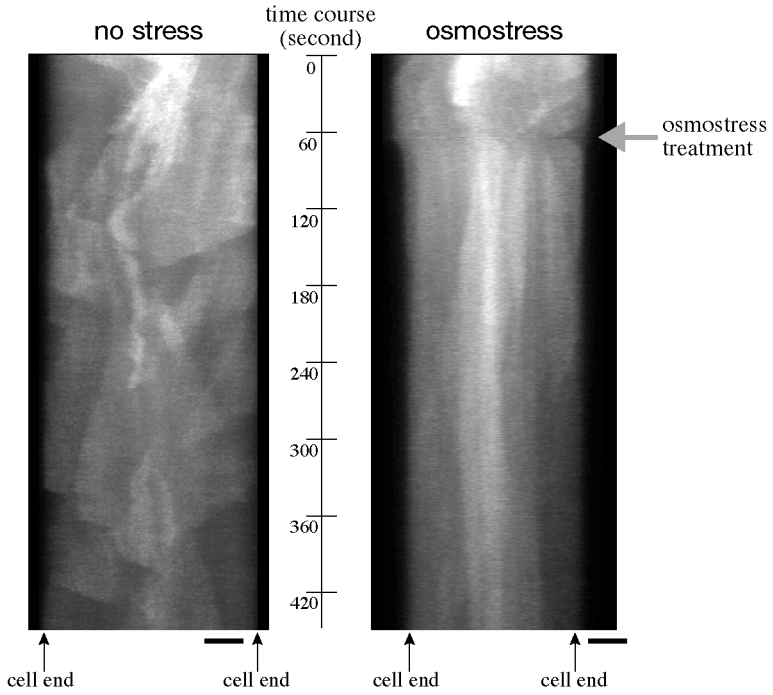
Table S1. *S. pombe* strains used in this study

Strain	Genotype	Source or reference
PR109	*h⁻*	Laboratory stock
CA6	*h⁻ his7-366 ade6-M216*	Laboratory stock
CA7	*h⁺ his7-366 ade6-M210*	Laboratory stock
CA14	*h⁻ spc1::ura4⁺*	Laboratory stock
CA2301	*h⁻ wsh3:GFP(ura4⁺)*	This study
CA2302	*h⁻ cdc25-22*	Laboratory stock
CA2307	*h⁻ wsh3:myc(ura4⁺)*	This study
CA2498	*h⁺ pom1::ura4⁺*	[7]
CA2520	*h⁻ pom1:GFP(KanMX6)*	[7]
CA2522	*h⁻ pom1:GFP(KanMX6) wsh3::ura4⁺*	This study
CA2525	*h⁻ wsh3:GFP(ura4⁺) nda3-KM311*	This study
CA2527	*h⁻ wsh3::ura4⁺*	This study
CA2548	*h⁻ tea1::ura4⁺*	[8]
CA2562	*h⁻ cdc11-132*	Laboratory stock
CA2569	*h⁻ cdc25-22 wsh3::ura4⁺*	This study
CA2634	*h⁻ nmt1:GFP:atb2(lys1⁺)*	Laboratory stock
CA2670	*h⁻ cdc11-132 wsh3::ura4⁺*	This study
CA2677	*h⁻ tea1:GFP(KanMX6)*	[9]
CA2735	*h⁻ tea1:GFP(KanMX6) wsh3::ura4⁺*	This study
CA2737	*h⁻ wsh3:GFP(ura4⁺) tea1::ura4⁺*	This study
CA3305	*h⁻ tea1:GFP(KanMX6) wsh3:HATAP(KanMX6)*	This study
CA3325	*h⁻ tea1::ura4⁺ spc1::ura4⁺*	This study
CA3341	*h⁻ pom1::ura4⁺ wsh3::ura4⁺*	This study
CA3345	*h⁻ tea1::ura4⁺ wsh3::ura4⁺*	This study
CA3349	*h⁻ win1:myc(ura4⁺) wsh3::ura4⁺*	This study
CA3742	*h⁻ wsh3:RFP(ura4⁺) tea1:GFP(KanMX6)*	This study
CA4005	*h⁻ wsh3:RFP(ura4⁺) nmt1:GFP:atb2(lys1⁺)*	This study
CA4023	*h⁻ tea1::ura4⁺ pom1::ura4⁺ wsh3::ura4⁺*	This study

All strains are *leu1-32 ura4-D18*.

References

1. Campbell, R.E., Tour, O., Palmer, A.E., Steinbach, P.A., Baird, G.S., Zacharias, D.A., and Tsien, R.Y. (2002). A monomeric red fluorescent protein. Proc Natl Acad Sci U S A *99*, 7877-7882.
2. Rigaut, G., Shevchenko, A., Rutz, B., Wilm, M., Mann, M., and Seraphin, B. (1999). A generic protein purification method for protein complex characterization and proteome exploration. Nat. Biotechnol. *17*, 1030-1032.
3. Sagolla, M.J., Uzawa, S., and Cande, W.Z. (2003). Individual microtubule dynamics contribute to the function of mitotic and cytoplasmic arrays in fission yeast. J. Cell Sci. *116*, 4891-4903.
4. Gustafsson, M.G. (2000). Surpassing the lateral resolution limit by a factor of two using structured illumination microscopy. J Microsc *198 (Pt 2)*, 82-87.
5. Agard, D.A., Hiraoka, Y., Shaw, P., and Sedat, J.W. (1989). Fluorescence microscopy in three dimensions. Methods Cell Biol *30*, 353-377.
6. Chen, H., Hughes, D.D., Chan, T.A., Sedat, J.W., and Agard, D.A. (1996). IVE (Image Visualization Environment): a software platform for all three-dimensional microscopy applications. J. Struct. Biol. *116*, 56-60.
7. Bähler, J., and Pringle, J.R. (1998). Pom1p, a fission yeast protein kinase that provides positional information for both polarized growth and cytokinesis. Genes Dev. *12*, 1356-1370.
8. Mata, J., and Nurse, P. (1997). tea1 and the microtubular cytoskeleton are important for generating global spatial order within the fission yeast cell. Cell *89*, 939-949.
9. Behrens, R., and Nurse, P. (2002). Roles of fission yeast tea1p in the localization of polarity factors and in organizing the microtubular cytoskeleton. J. Cell Biol. *157*, 783-793.



Supplemental Figure-1 Tatebe *et al.*